5196 *Macromolecules* **2009**, *42*, 5196–5207
DOI: 10.1021/ma9004154

Macromolecules
ARTICLE

Study of Glass Transition and Reinforcement Mechanism in Polymer/Layered Silicate Nanocomposites

Xingui Zhang and Leslie S. Loo*

School of Chemical and Biomedical Engineering, Nanyang Technological University, Singapore 637459, Singapore

Received February 24, 2009; Revised Manuscript Received June 6, 2009

ABSTRACT: The structure−property relationship of polymer/layered silicate nanocomposites was investigated in this study. Polymer nanocomposites based on completely amorphous poly(hexamethylene isophthalamide) with exfoliated, intercalated, or agglomerated nanoclay morphology were produced and analyzed by X-ray diffraction and transmission electron microscopy. Differential scanning calorimetry measurements were used to characterize the glass-transition behavior. Dynamic mechanical analysis was performed to investigate the nature of the constrained region as the reinforcement mechanism. The modulus enhancement of the organoclay nanocomposites was found to have good linear correlation with the volume of the constrained region. The type of polymer−nanofiller interaction strongly influences the amount and modulus of the constrained region, and both of the latter contribute to the enhancement in the storage modulus of the polymer nanocomposite. The mechanical properties of the constrained region are temperature-dependent. Constrained region models for polymer nanocomposites were proposed on the basis of these results. The constrained volume in amorphous polymer nanocomposites was found to be much less than that in semicrystalline systems.

1. Introduction

In recent years, polymer/nanoclay nanocomposites have generated much research interest because of their enhanced properties at lower nanofiller loading as compared with conventional micrometer-size fillers.[1−3] For instance, the addition of 5 wt % montmorillonite clay to nylon 6 has led to remarkable improvements in mechanical properties[4] and heat distortion temperature.[5] Such property enhancements have been attributed to a significant volume of polymer chains that were constrained because of their interactions with the well-dispersed clay layers.[6,7] An understanding of the underlying molecular structure and dynamics is therefore critical to predict macroscopic properties and to design polymer nanocomposites with desired characteristics.

Differential scanning calorimetry (DSC) is an important technique that is used to study the glass transition and chain mobility in polymer/nanoclay nanocomposites.[8−11] In such systems, two distinct types of dynamic behavior have been reported in the literature. One is the slower relaxation dynamics associated with higher glass-transition temperature (T_g), which has been observed in some exfoliated or intercalated polymer/clay nanocomposites.[12,13] This behavior has been attributed to the large interlayer distance and the strong polymer−filler interactions that exist in these systems.[9,14] In contrast, when the average clay layer distance is less than the characteristic correlation length of polymer chains for relaxation, such as in intercalated nanoclay systems, the intercalated polymer segments will exhibit the faster relaxation mode, thereby leading to depressed T_g or the absence of cooperative glass transition.[8,10,15] Moreover, it was observed that the plasticization effect of organic surfactants on nanoclay would also result in the reduction in T_g.[16−18]

In the polymer/nanoclay systems, the restrictive environment of the polymer chains inside the clay gallery will greatly affect not only the molecular relaxation and mobility but also their crystallization.[7,8,19] To remove the complications that would arise because of the presence of a crystalline phase or nanoclay-induced crystalline phase transitions,[7,20] the glass-transition behavior of nanocomposites based on amorphous polymer, such as polystyrene (PS) and poly(methyl methacrylate) (PMMA), has been extensively studied.[3,10,21,22] However, because of the low polarity of these polymer matrices, most nanocomposites based on amorphous polymers tended to form intercalated structures.[23,24] The polymer dynamics of exfoliated amorphous polymer/clay hybrids has yet to be investigated in detail.

Dynamic mechanical analysis (DMA) has also been used extensively to investigate chain mobility in viscoelastic materials.[2,25,26] For nylon 6/nanoclay nanocomposites, DMA analysis has shown that the addition of 5 wt % nanoclay has resulted in a large increase in the volume percent of the constrained region from 33% (in the homopolymer) to 70% in the polymer nanocomposite.[27] However, many reports of calculated constrained volume induced by nanoclay have been based on semicrystalline polymers or cross-linked rubbers but not on fully amorphous polymers.[2,7,28] Recently, Adame and Beall used atomic force microscopy (AFM) to measure the constrained region in amorphous polyamide/nanoclay nanocomposites.[29] Furthermore, the nature of the constrained region as the reinforcement mechanism has not yet been studied in detail for polymer/nanoclay systems.

In a recent paper, we prepared a novel amorphous polyamide/montmorillonite nanocomposite based on poly(hexamethylene isophthalamide) by melt intercalation.[30] By suitable choice of organoclay, well-exfoliated morphologies had been achieved in this system. The improvement in Young's modulus was comparable to semicrystalline aliphatic nylon 6 nanocomposites. Therefore, this amorphous polymer nanocomposite system can be used as a model compound to develop some fundamental theories in polymer nanocomposites.

The present article serves to accomplish three objectives: (a) to characterize the glass-transition behavior of an amorphous

*Corresponding author. Tel: 65- 6790-6737. Fax: 65- 6794-7553. E-mail: ssloo@ntu.edu.sg.

 Published on Web 07/02/2009

Table 1. Materials Used in This Study

material (designation used in this article)	supplier designation	specifications
aPA	Durethan T40	poly(hexamethylene isophthalamide)
NaMMT	Cloisite Na^+	92.6 CEC, d_{001} spacing = 1.05 nm[a]
30BMMT	Cloisite 30B: methyl, tallow, bis-2-hydroxyethyl quaternary ammonium chloride organoclay	90 CEC, organic content = 28.4 wt %, d_{001} spacing = 1.84 nm
10AMMT	Cloisite 10A: dimethyl, benzyl, hydrogenated tallow quaternary ammonium chloride organoclay	125 CEC, organic content = 36.9 wt %, d_{001} spacing = 1.95 nm
20AMMT	Cloisite 20A: dimethyl, dihydrogenated tallow quaternary ammonium chloride organoclay	95 CEC, organic content = 38.1 wt %, d_{001} spacing = 2.42 nm

[a] CEC: cation exchange capacity, mequiv/100 g.

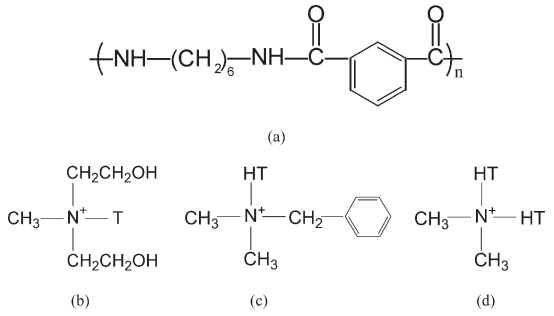

Figure 1. Chemical structures of (a) aPA polymer, (b) surfactant on 30BMMT, (c) surfactant on 10AMMT, and (d) surfactant on 20AMMT.

polymer/nanoclay nanocomposite system, (b) to investigate the mechanical properties of the constrained volume fraction and demonstrate its role in the mechanical reinforcement of polymer nanocomposites, and (c) to propose a model to highlight the differences in the nature of the constrained region for nanocomposites based on semicrystalline polymers, cross-linked rubbers, and amorphous polymers.

2. Experimental Section

2.1. Materials. The materials used in this study are described in Table 1. The amorphous polyamide (aPA) was obtained from Lanxess under the product trade name Durethan T40. Pristine sodium montmorillonite (MMT) nanoclay and three types of MMT-based organoclay were supplied by Southern Clay Products. They are abbreviated as NaMMT, 30BMMT, 10AMMT, and 20AMMT, respectively. The chemical structures of the polymer and the surfactants are shown in Figure 1, where "T" and "HT" stand for tallow and hydrogenated tallow, respectively. Prior to the blending of the polymer and nanoclay, they were first dried in a vacuum oven at 80 °C for at least 12 h.

2.2. Preparation of Polymer Nanocomposites. The polymer/clay nanocomposites were prepared via a two-step process under a nitrogen atmosphere according to the method described in a previous paper.[30] First, a 50 g master batch of the dried polymer pellets containing 12 wt % MMT (wt % excludes surfactants) was prepared by melt blending in a Haake Polydrive mixer at 270 °C. The average residence time was 5 min. Appropriate amounts of dried aPA pellets were then blended with the master batch to obtain polymer nanocomposites with the requisite MMT content using the same mixer at a lower temperature of 260 °C with a similar residence time. For aPA containing organoclay, polymer nanocomposites with nominal content of 2, 5, 7, and 10 wt % MMT (wt % excludes surfactants) were prepared. For aPA containing NaMMT, only samples containing 5 and 10 wt % MMT were made. We made pure aPA samples by simply blending the dried polymer pellets in the first blending process at 270 °C. Finally, the pure aPA and the polymer nanocomposites were compressed into films (ca. 150 ± 5 μm) at 220 °C using a Carver Press (model 4128) for later characterizations. In addition, for dynamic mechanical measurements, specimens of approximately 1.1 mm in thickness were formed by compression molding.

2.3. Characterization. Wide-angle X-ray diffraction (WAXD) measurements were performed at room temperature on a Siemens D5005 X-ray diffractometer using Cu Kα radiation ($\lambda = 0.1542$ nm). The scanning rate was 1°/min for values of 2θ between 1 and 10°.

TEM was used to observe the dispersion of clay layers in the polymer matrix. Thin sections of approximately 50 nm in thickness were cut from the nanocomposites at room temperature and examined using a JEOL 3010 TEM instrument at an acceleration voltage of 200 kV.

DSC measurements were carried out under a nitrogen gas atmosphere in a Mettler Toledo DSC 822 analyzer. The samples were first heated to 280 °C (to remove any previous processing history), then cooled to 30 °C, and finally heated to 280 °C again. The heating and cooling rates for all runs were 10 °C/min. Both the glass-transition temperature (T_g) and heat capacity (C_p) were obtained from the reversible heat flow curve. T_g is determined according to ASTM E1356-08, and C_p is determined from the software STAR^e Thermal Analysis.[21]

The thermal−mechanical behavior of the nanocomposites was examined using a Research Instrument RSA III DMA instrument using a three-point bend mode. Experiments were carried out on test specimens approximately 40 mm in length, 12 mm in width, and 1.1 mm in thickness. Specimens were heated from 30 to 160 °C at a rate of 2 °C/min and simultaneously analyzed for storage modulus (E'), loss modulus (E''), and tan δ at a frequency of 1 Hz. The heat distortion temperature (HDT) for these materials was estimated from plots of log E' versus temperature using the technique developed by Scobbo.[31] According to this method, for amorphous polymer and its composites, the HDT is taken as the value of the temperature corresponding to a stress of 0.45 MPa (or log $E' = 8.3$).

3. Results and Discussion

3.1. Morphology of Amorphous Polyamide/Nanoclay Nanocomposites. The morphology of aPA/30BMMT and aPA/10AMMT polymer nanocomposites has been reported in a previous publication.[30] For all aPA/30BMMT nanocomposites containing up to 10.54 wt % MMT, WAXD results showed a featureless profile devoid of peaks for values of 2θ from 1 to 10°, and TEM images showed well-dispersed single clay layers. This indicates that fully exfoliated nanoclay morphology was present in aPA/30BMMT nanocomposites.[30] Figure 2a shows a representative TEM image for aPA/30BMMT nanocomposite containing 7.23 wt % MMT. It is seen that the nanoclay platelets have been fully delaminated and are well-dispersed in the polymer matrix. Similarly, for aPA/10AMMT nanocomposites, WAXD and TEM data also indicated fully exfoliated MMT morphology for nanoclay content up to 6.99 wt %. (The only exception was aPA/10AMMT hybrids containing 10.65 wt % MMT, which showed intercalated MMT morphology).[30] Figure 2b

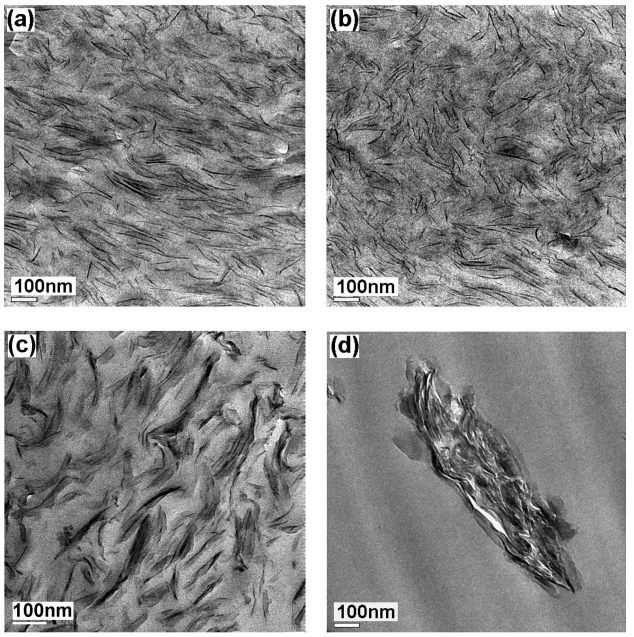

Figure 2. TEM images of (a) aPA/30BMMT containing 7.23 wt % MMT, (b) aPA/10AMMT containing 6.99 wt % MMT, (c) aPA/20AMMT containing 7.25 wt % MMT, and (d) aPA/NaMMT containing 5.03 wt % MMT.

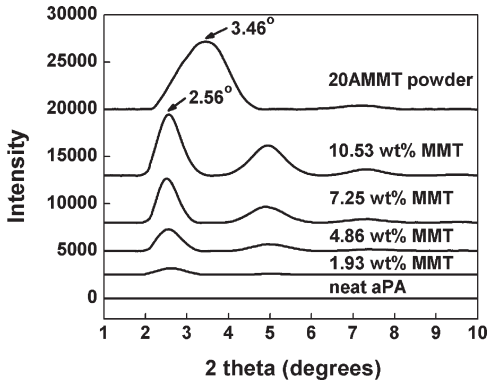

Figure 3. WAXD patterns of aPA/20AMMT nanocomposites.

shows a representative TEM image for aPA/10AMMT nanocomposite containing 6.99 wt % MMT. It can be seen that the nanoclay platelets have also been fully delaminated and are randomly dispersed. The presence of exfoliated morphologies in both aPA/30BMMT and aPA/10AMMT systems has been attributed to the favorable interactions that exist between the surfactants and the polyamide molecules: the hydroxyl groups in 30BMMT can form hydrogen bonds with aPA, whereas the phenyl groups in 10AMMT can interact with the aromatic groups in aPA through van der Waals forces.[23,30]

The morphology of aPA/20AMMT polymer nanocomposites has not been reported elsewhere and will be presented in this article. Figure 3 shows the WAXD patterns of the nanocomposites with different MMT content. Pure 20AMMT powder has a prominent basal reflection at $2\theta = 3.46°$, corresponding to a d spacing of 2.42 nm. All aPA/20AMMT nanocomposites have a prominent basal peak at $2\theta = 2.56°$ that corresponds to a larger d spacing of 3.45 nm, suggesting the presence of an intercalated structure. Figure 2c shows a representative TEM image of aPA/20AMMT nanocomposite containing 7.25 wt % MMT. It reveals the existence of both intercalated and exfoliated nanoclay structures. The ordered clay arrangement of the intercalated structure gives rise to the peak at $2\theta = 2.56°$ in Figure 3. In contrast with 30BMMT and 10AMMT, the surfactant in organoclay 20AMMT lacks suitable organic groups to form favorable interactions with aPA chains, thereby resulting in intercalated nanoclay morphology.

The morphology of aPA/NaMMT nanocomposites has also been previously reported.[30] Both TEM and WAXD results have shown that the clay particles agglomerated in the polymer matrix regardless of the nanoclay concentration. This can be clearly seen from the TEM image of the hybrid containing 5.03 wt % MMT in Figure 2d. The poor dispersion of the nanofiller has been attributed to the absence of surfactants on NaMMT.[30]

Therefore, we have a polymer nanocomposite system with three different kinds of nanoclay morphology depending on the nature of the organoclay used: agglomerated (aPA/NaMMT), intercalated (aPA/20AMMT), and exfoliated (aPA/30BMMT and aPA/10AMMT). The only exception is aPA/10MMT containing 10.65 wt % MMT, which has intercalated nanoclay morphology. In the following discussions, we will use DSC and DMA to study the polymer chain relaxation behavior and mobility in the vicinity of the glass transition in view of these different nanocomposite morphologies.

3.2. Glass-Transition Behavior. Polymer molecules are sensitive to the local environment because of the characteristic long-chain morphology.[9,32] Therefore, the values of T_g and normalized change of heat capacity (ΔC_p) of a polymer at glass transition are important parameters that provide information about the structural changes undergone by the polymer during the transition.[33]

3.2.1. T_g of aPA Nanocomposites. Figure 4 shows the normalized DSC traces in the glass-transition region for pure aPA and all polymer nanocomposites. The value of T_g for all specimens was determined from the midpoints of the corresponding glass-transition region, as shown by the topmost curve in Figure 4a. The T_g of pure aPA is 121.4 °C, which is similar to the value of 123 °C obtained by Hu et al.[34] Nanoclay is known to induce phase transitions in some polymer systems (e.g., nylon 6) by providing nucleation sites.[35−37] In this study, no other transitions are observed in all samples, thereby indicating that both the homopolymer and the nanocomposites are completely amorphous and do not contain crystalline regions. This allows us to analyze the polymer nanocomposite systems without the complicating effects of crystalline phase. Figure 5 shows the measured T_g values plotted as a function of MMT content.

Figures 4a and 5 show the changes in the glass-transition region for the exfoliated aPA/30BMMT system. Unlike the monotonic increase or decrease in T_g with increasing nanoclay content that has been observed in some nanocomposite systems,[9,38] the T_g behavior of aPA/30BMMT nanocomposites is quite complicated. At the low filler concentration of 2.10 wt %, T_g increases to the value of 124.0 °C. As MMT content increases further, it is observed that the value of T_g decreases, and the intensity of the glass transition becomes shallower, as seen in Figure 4a. When the MMT content is 10.54 wt %, T_g decreases to a value of 119.9 °C.

A similar trend in T_g behavior is also observed for the exfoliated aPA/10AMMT nanocomposites with MMT content below 10.65 wt %, as shown in Figure 4b and Figure 5. However, for the aPA/10AMMT nanocomposite with 10.65 wt % MMT, which contains the intercalated nanoclay morphology, there is a sharp decrease in T_g (117.6 °C). This is in contrast with the completely exfoliated aPA/30BMMT

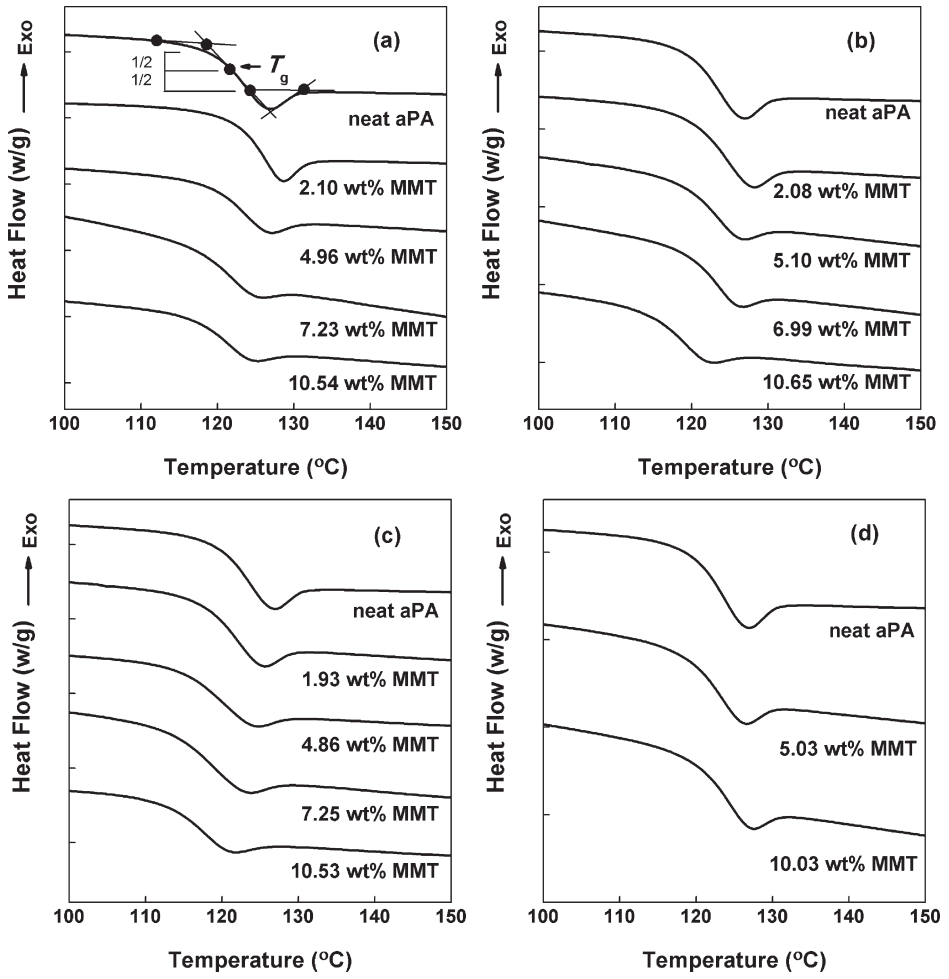

Figure 4. DSC curves in the glass-transition region of (a) aPA/30BMMT, (b) aPA/10AMMT, (c) aPA/20AMMT, and (d) aPA/NaMMT nanocomposites.

system, whose T_g decreases in a fairly linear fashion from 2.10 to 10.54 wt %.

Figures 4c and 5 show the glass-transition behavior of the intercalated aPA/20AMMT nanocomposites. It is observed that T_g exhibits a monotonic and linear decrease from 121.4 to 115.5 °C with increasing nanoclay content.

Recent studies have shown that the relaxation mode depended not only on the extent of nanoclay dispersion but also on the strength of interactions between filler and polymer matrix.[9,13,21] For instance, in an intercalated epoxy/nanoclay system composed of the diglycidyl ether of bisphenol A cured by stoichiometric amounts of 4,4′-diaminodiphenyl sulfone anchored onto MMT, T_g increased monotonically up to 7 °C with increasing MMT content up to 10 phr (per hundred resin).[9] However, the depressed T_g observed in intercalated PS nanocomposites has been attributed to nonpolar PS chains exhibiting weak interactions with nanoclay layers.[3,21]

The primary intermolecular interaction occurring in aPA homopolymer is hydrogen bonding between the amide N−H and C=O groups.[39] In intercalated aPA/20AMMT hybrids, as nanofiller content increases, more polymer chains are confined between clay galleries.[40] This will disrupt the stable intermolecular structure of aPA matrix. Therefore, the steady depression in T_g with increasing clay concentration can be attributed to the fast relaxation behavior[3,41] of the intercalated chains and the plasticizing effect of the organic modifier in the organoclay.[16,17]

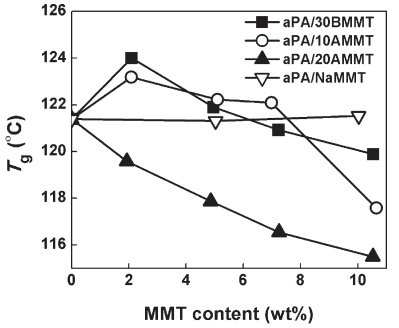

Figure 5. Values of T_g as a function of clay content in aPA/clay nanocomposites.

However, in the well-dispersed aPA/30BMMT and aPA/10AMMT nanocomposites, the increase in T_g observed at low clay concentration (2 wt % MMT) can be attributed to the effective interactions between the organoclay and aPA chains,[9,13] that is, hydrogen bonding in aPA/30BMMT and polarity compatibility in aPA/10AMMT. However, at higher filler loadings, because of the plasticization effect due to the organic surfactants, the values of T_g will decrease with increasing clay content. A similar phenomenon has also been observed in fully exfoliated nylon 6/clay nanocomposites, where the DSC results showed a slight decrease in T_g with the addition of nanoclay.[7,42] The large drop in T_g observed for aPA/10AMMT nanocomposite with 10.65 wt % MMT is

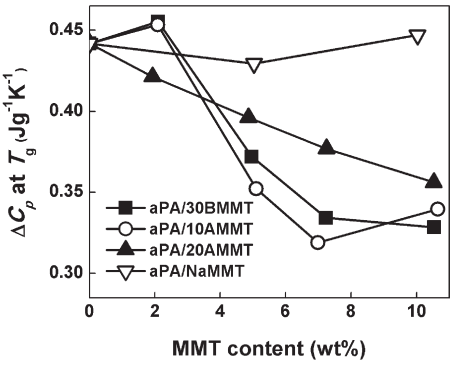

Figure 6. Normalized change in heat capacity (ΔC_p) of the polymer at glass transition as a function of nanoclay content in aPA nanocomposites.[10]

largely attributed to structural confinement because of the presence of the intercalated morphology.[8,43]

Figures 4d and 5 show that both the aggregated aPA/NaMMT hybrids have similar onset temperature, T_g, and end temperature as the homopolymer. It indicates that the clay agglomerates do not significantly affect the glass-transition behavior of bulk polymer, and only the organic surfactants show the plasticization effect.[16,44]

It is known that the value of T_g also depends on polymer molecular weight.[19] The glass-transition temperature generally increases with molecular weight (M_n), and there exists a critical value for M_n beyond which T_g reaches an asymptotic value, $T_g(\infty)$.[21,45] It has been shown that among all aPA/nanoclay nanocomposites used in this study, the largest reduction in M_n was found in aPA/NaMMT containing 10.03 wt % MMT.[30] However, the T_g of this particular hybrid is 121.5 °C, similar to that of the homopolymer. Therefore, the molecular weights of the polymer in all the nanocomposites used in this study were above the critical value, and the glass-transition behavior would not be significantly influenced by this variable.

3.2.2. ΔC_p at Glass Transition of Amorphous Polyamide Nanocomposites. The value of the heat capacity is proportional to the number of internal degrees of freedom of molecular motion.[11] Therefore, the normalized change of heat capacity (ΔC_p) at glass transition of the polymer nanocomposites, which strongly depends on the nanoclay morphology,[21] would allow us to determine the changes in polymer chain mobility in the nanocomposites directly. Figure 6 shows the effect of nanoclay on ΔC_p at glass transition in aPA nanocomposites. The value of ΔC_p is 0.44 J g^{-1} K^{-1} for neat aPA.

From Figure 6, it is observed that for aPA/20AMMT nanocomposites, ΔC_p at glass transition decreases monotonically with filler content. As more nanofiller was introduced into the nanocomposite system, more polymer chains would be confined between nanoclay galleries. This would decrease the number of degrees of freedom for the polymer segments,[11] thereby causing ΔC_p to decrease with increasing nanoclay content. This is consistent with the results of Li et al., who have observed that in the intercalated PS/organoclay system, when the PS content was below 30 wt %, the value of ΔC_p for the nanocomposites was close to zero, indicating the absence of cooperative glass transition.[8] As polymer concentration was increased further, ΔC_p increased drastically. The results of Li et al. also suggested that the polymer chains confined within clay galleries in intercalated systems would not contribute to ΔC_p.[21]

In contrast, Figure 6 shows that for both the exfoliated aPA/30BMMT and aPA/10AMMT systems, ΔC_p at the glass transition first exhibits a slight increase at 2 wt % MMT. However, at higher clay loadings, ΔC_p is observed to decrease with increasing nanoclay content, and it decreases at a higher rate compared with the intercalated aPA/20AMMT system. A similar trend has also been observed in fully exfoliated nylon 6/nanoclay system,[46] in which ΔC_p at the glass transition showed a slight increase up to 5 wt % clay, after which it would continuously decrease with increasing clay content up to 35 wt % nanoclay.

These results indicate that for exfoliated systems the molecular motions of polymer chains would not be appreciably affected when the amount of nanoclay in the nanocomposite is low. However, at higher clay contents, the increasing amount of restricted polymer chains in the nanocomposites would reduce ΔC_p to values lower than that of the homopolymer. Moreover, for any given clay content, the polymer−nanoclay contact area (and hence the amount of restricted polymer chains) would be larger for exfoliated systems than for intercalated systems, and hence the value of ΔC_p would be lower for the former.[47] This is consistent with the data in Figure 6, which shows that the values of ΔC_p for aPA/30BMMT and aPA/10AMMT are lower than those for aPA/20AMMT at high clay loadings. The only anomaly in Figure 6 is that the aPA/10AMMT nanocomposite with 10.65 wt % MMT has a larger ΔC_p value than aPA/10AMMT with 6.99 wt % MMT. This can be attributed to the intercalated morphology that was observed in the former.

Figure 6 also shows that the ΔC_p of aPA/NaMMT hybrids is similar to that of the pure polymer, indicating that the nanoclay agglomerates do not significantly alter the mobility of polymer chains at glass transition.[21] This is due to poor polymer−nanoclay interactions and the absence of polymer intercalation into the clay galleries.

From these results, it can be seen that the values of ΔC_p exhibit variable trends depending on the state of clay dispersion in the polymer nanocomposites. Therefore, it can be conveniently used to indicate the approximate inherent interfacial adhesion in polymer/nanoclay systems.[46]

In summary, it is clear that the intercalated aPA/20AMMT nanocomposites show the typical fast relaxation associated with depressed T_g. However, the relaxation behavior of the exfoliated aPA/30BMMT and aPA/10AMMT systems does not fit into the normal models as expected. The depressed value of ΔC_p in both the intercalated and exfoliated systems indicates that the interactions between polymer molecules and organoclay layers do restrict the chain mobility. DMA measurements were then carried out to determine the amount of constrained polymer chains in each of the nanocomposites.

3.3. Dynamic Mechanical Analysis Measurements. DMA measurements can be used to detect changes in the molecular mobility between polymer segments in the vicinity of nanoclay and to evaluate the stiffness of the nanocomposites.[48] Figure 7 shows the effect of nanoclay type and content on the storage modulus (E') of aPA/nanoclay systems. The values of normalized E' at 30, 100, and 130 °C for all samples are listed in columns 2, 3, and 4 of Table 2. Figure 7a,b,c shows that in all aPA/organoclay systems, E' increases gradually with increasing filler content for all temperatures. In contrast, Figure 7d indicates that the aPA/NaMMT hybrid shows an increase in E' only at temperatures below T_g but not above T_g. Table 2 shows that for a given nanofiller content the organoclay 10AMMT produced the highest degree of storage modulus enhancement among all nanocomposites (for the three temperatures listed). Furthermore,

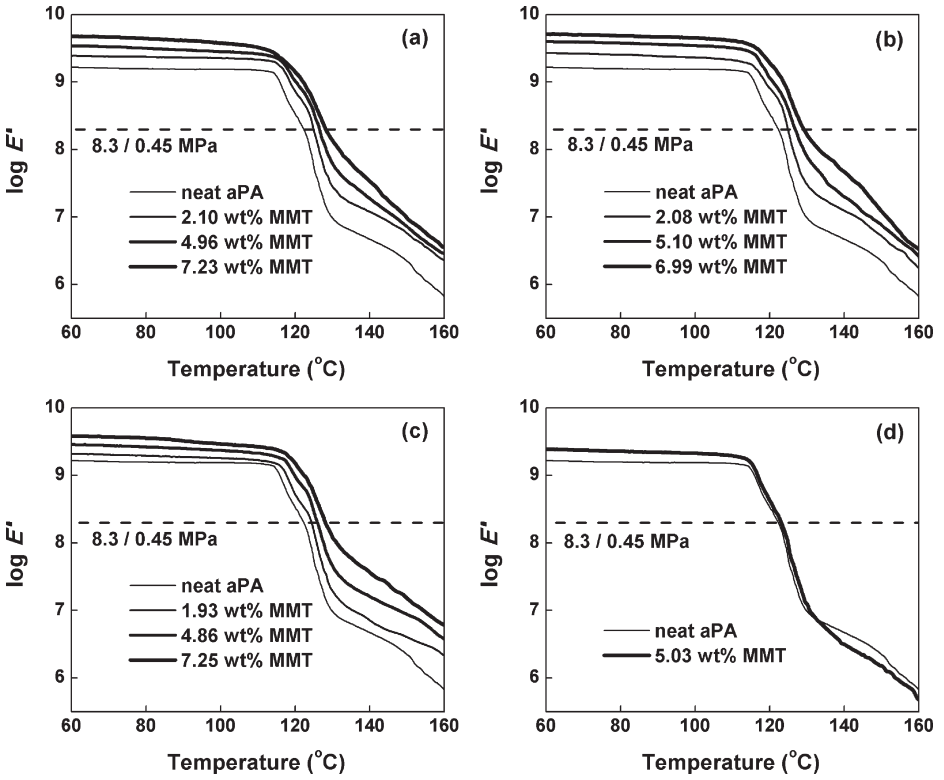

Figure 7. Storage modulus E' spectra for (a) aPA/30BMMT, (b) aPA/10AMMT, (c) aPA/20AMMT, and (d) aPA/NaMMT nanocomposites. The technique used for estimating HDT is illustrated in the plot of log E' versus temperature.[31]

Table 2. Values of E', HDT, and the Volume Fraction of Constrained Region in aPA and Its Nanocomposites

sample	normalized E' (30 °C)[a]	normalized E' (100 °C)[a]	normalized E' (130 °C)[a]	HDT (°C)	C
aPA (Durethan T40)	1.00	1.00	1.00	122.3	0
aPA/30BMMT[b,c]					
2.10 wt %	1.38	1.46	2.73	124.9	0.0292
4.96 wt %	1.93	1.81	6.08	126.5	0.0623
7.23 wt %	2.70	2.42	13.32	128.3	0.1174
aPA/10AMMT[b,c]					
2.08 wt %	1.46	1.49	2.97	125.0	0.0314
5.10 wt %	2.21	2.25	7.65	126.8	0.0884
6.99 wt %	2.84	2.91	15.81	129.1	0.1207
aPA/20AMMT[b,c]					
1.93 wt %	1.18	1.16	1.88	124.4	0.0156
4.86 wt %	1.60	1.52	4.45	126.0	0.0553
7.25 wt %	2.09	1.89	11.78	128.1	0.0983
aPA/NaMMT[b,c]					
5.03 wt %	1.40	1.38	1.15	123.1	N/A[d]

[a] Normalized E' is the ratio of the value E' of the nanocomposite to the value of E' of aPA homopolymer obtained at the same temperature. [b] Clay contents are based on MMT only. [c] No mechanical tests were carried out on samples with around 10 wt % MMT because they were too brittle. [d] No constrained region exists in aPA/NaMMT system.

for all aPA/organoclay nanocomposites, the greatest reinforcing effect occurred above the glass transition. It has also been reported that for nylon 6/nanoclay nanocomposites, better modulus enhancement was achieved at temperatures above T_g.[49] This phenomenon indicates that the organoclay reinforcement imposes the stable constrained region in polymer segments.[50]

3.3.1. Heat Distortion Temperature of Amorphous Polyamide Nanocomposites. The mechanical reinforcement of polymer nanocomposites leads not only to modulus enhancement but also to an increase in HDT.[51] DMA results can be conveniently used to estimate the HDT of polymers or polymer nanocomposite systems.[31,49,52] Figure 7 illustrates how the HDT was estimated using E' data, and the values of HDT are listed in column 5 of Table 2. It is observed that the HDT of all aPA/organoclay nanocomposites increases with increased MMT content. Moreover, at similar MMT loadings, aPA/10AMMT nanocomposites exhibit the highest HDT among all hybrid systems. In contrast, the HDT of aPA/NaMMT hybrid with 5.03 wt % MMT is only about 1 °C higher than that of neat aPA.

For the amorphous polymer/clay hybrids used in this study, the increase in HDT was not as dramatic as that for other polymer/nanoclay nanocomposites based on semicrystalline polymers.[52] For instance, the HDT of exfoliated nylon 6/clay increased from 58 to 150 °C at 4.6 wt % MMT loading, as measured by DMA.[49] The HDT of intercalated polypropylene/clay also increased by about 50 °C at a clay content of 9 wt %.[51] The reason is that nanoscale clay would exert a shielding effect on molecular chains, which are subjected to external heat and distortion.[53] For semicrystalline polymers, this shielding effect

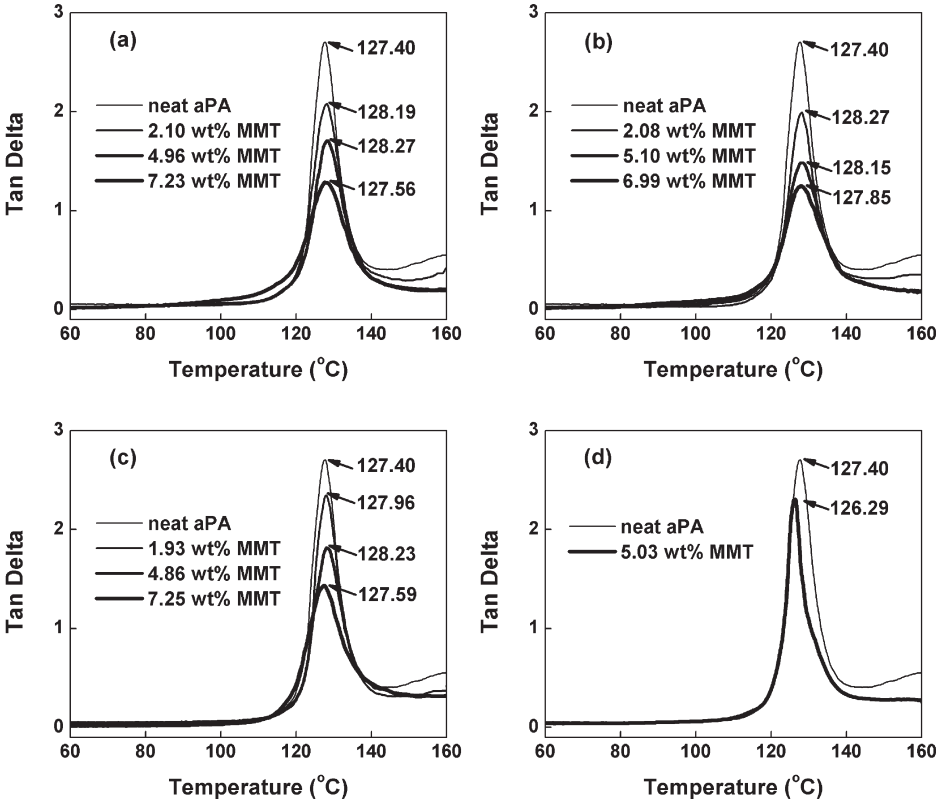

Figure 8. tan δ spectra for (a) aPA/30BMMT, (b) aPA/10AMMT, (c) aPA/20AMMT, and (d) aPA/NaMMT nanocomposites.

serves to stabilize the crystalline phase until the external temperature reaches the melting point of the bulk polymer, so HDT would increase from a value near T_g to a value close to the melting point of the polymer crystals.[54] However, for an amorphous polymer and its composites, the shielding effect would not be as effective because of the absence of the crystalline regions. Therefore, the values of HDT would not increase very much beyond T_g.[55]

3.3.2. Constrained Region in Amorphous Polyamide Nanocomposites. During the glass transition, the long-range polymer chains gain mobility and thus dissipate a great amount of energy through viscous movement. This is shown in the tan δ peak in a DMA test.[2] The temperature at the maximum value of tan δ peak was often regarded to be the value of T_g.[56,57] However, Nielsen et al. stressed that the temperature at maximum damping was not T_g, although it could be close to T_g. This maximum point of tan δ peak was much more sensitive to parameters such as filler content or blend morphology than T_g itself.[55] The height depression in the tan δ peak indicates that there is a reduction in the amount of mobile polymer chains during the glass transition and hence can be used to estimate the amount of constrained chains.[57]

Figure 8 shows the tan δ curves for all of the different nanoclay types and concentration. There is only a single tan δ loss peak observed for all the samples, again indicating the wholly amorphous nature of the polymer nanocomposites.[58,59] This is consistent with DSC data. From Figure 8a,b,c, it is observed that for all aPA/organoclay nanocomposites there is a slight shift in the tan δ peak toward higher temperature compared with the pure polymer. For each type of organoclay, it is also observed that the addition of more nanofillers resulted in a decrease in the magnitude of the tan δ peak but an increase in its peak width, indicating the restricted mobility of polymer chains and the broader distribution of relaxation times in the aPA nanocomposites.[57]

Figure 8d shows that the addition of pristine clay caused the loss tangent peak to become narrow and to shift to a lower temperature. This reflects the heterogeneity of clay dispersion in the phase-incompatible hybrid.[56] Therefore, no nanoscale constrained region exists in the aPA/pristine clay system.

Both DSC and DMA studies suggest that some portions of polymer chains become immobilized in aPA/organoclay nanocomposites at high clay loadings (depressed ΔC_p and depressed tan δ peak), whereas the presence of pristine clay does not significantly restrict the chain mobility on the nanoscale level. However, there is a slight difference in the data provided by these two techniques, particularly for the two exfoliated systems. The DSC data indicated that at low filler content, that is, 2 wt % MMT, the mobility of polymer chains in aPA/30BMMT and aPA/10AMMT would not be affected, as evidenced by the increased ΔC_p. On the other hand, DMA results showed that the addition of a small amount of organoclay in these two systems would restrict the chain mobility, as seen by the diminished tan δ peak. Because DSC analyzes thermal−dynamic behavior, whereas DMA measures thermal−mechanical deformation, these differences are attributed to the different sensitivities of the molecular segments to these two techniques.[2,8]

To understand the role of the constrained region in enhancing the mechanical properties of the nanocomposites, it is important to determine quantitatively the volume fraction of these regions in aPA/organoclay nanocomposites. Rheological measurements showed that aPA nanocomposites exhibited linear viscoelasticity even at high nanofiller content, that is, 7 wt % MMT.[60] For linear viscoelastic behavior, the relationship among the energy loss fraction of the polymer nanocomposite W and tan δ is given by the

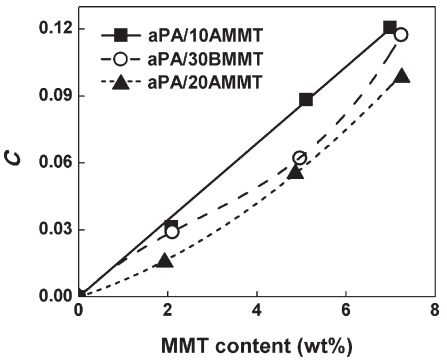

Figure 9. Graphs of C versus MMT content for aPA/10AMMT, aPA/30BMMT, and aPA/20AMMT nanocomposites. The lines are the best fit curves.

following equation[6,27]

$$W = \frac{\pi \tan \boldsymbol{\delta}}{\pi \tan \boldsymbol{\delta} + 1} \tag{1}$$

The energy loss fraction W at the tan δ peak is expressed by the dynamic viscoelastic data in the form

$$W = \frac{(1 - C) W_0}{1 - C_0} \tag{2}$$

where C is the volume fraction of the constrained region, $(1 - C)$ is the fraction of the amorphous region, and W_0 and C_0 denote the energy fraction loss and volume fraction of the constrained region for pure aPA, respectively. This equation can be rearranged as follows

$$C = 1 - \frac{(1 - C_0) W}{W_0} \tag{3}$$

The energy loss fraction at tan δ peak is obtained at the frequency of 1 Hz, and the value of C_0 is taken to be 0 (totally amorphous phase in aPA matrix). The height of the tan δ peak is used to calculate W according to eq 1.[6,7,50] The fraction of the constrained region of aPA/clay nanocomposites can then be estimated from eq 3.

The last column in Table 2 lists the values of C for each sample, and Figure 9 shows the plots of the volume fraction of the constrained region versus MMT content for the three aPA/organoclay systems. It is observed that at similar MMT concentrations, the volume fraction of the constrained region in both of the exfoliated systems (aPA/30BMMT and aPA/10AMMT) is higher than that of the intercalated aPA/20AMMT system. This is due to two factors. First, the exfoliated clay morphology generates a larger contact area between the nanoclay surface and polymer chains, thereby resulting in a larger amount of constrained region.[47] Second, the enhanced interfacial attraction between 10AMMT or 30BMMT and aPA matrix results in a larger quantity of C in these nanocomposites compared with aPA/20AMMT.

The amount of constrained region in aPA/10AMMT is observed to be higher than that in aPA/30BMMT at a given MMT content, even though the nanoclay is well-dispersed in both systems. This indicates that there is stronger interaction between aPA and 10AMMT. The different types of polymer−organoclay interaction have been investigated by using Fourier transform infrared (FTIR) spectroscopy.[60] The FTIR results showed the more stable molecular structure of the aPA matrix upon the introduction of organoclay 10AMMT.[23] This is due to the enhanced cohesive van der Waals attractions between the phenol rings in 10AMMT and the aromatic moieties in the polymer. However, in the aPA/30BMMT system, although hydrogen bonding could exist between aPA and 30BMMT surfactant, this would also reduce the self-associated hydrogen bonds between the polymer chains and influence the primary intermolecular structure.[61]

Figure 9 also shows that for the aPA/10AMMT system, there is a linear relationship between C and MMT content; however, in aPA/30BMMT and aPA/20AMMT systems, the constrained volume varies with the amount of nanofiller in a cubic and quadratic manner, respectively. Therefore, the fraction of constrained region in a polymer nanocomposite will depend not only on the filler content but also on the nature of the polymer−filler interaction.

3.3.3. Proposed Models of Constrained Region in Polymer Nanocomposites. It was reported by many researchers that a small amount of clay would immobilize a significant amount of polymer chains during the glass transition.[2,7,27,28] Besides the extensively studied nylon 6/nanoclay system,[27] DMA measurements have also showed that the addition of 5 wt % nanoclay in an intercalated latex copolymer resulted in an increase in constrained volume from 0 to 50%.[2] Furthermore, Utracki et al. have investigated the pressure−volume−temperature (PVT) behavior of several polymer/nanoclay systems.[62−64] They reported that the incorporation of 1.6 wt % nanoclay reduced the free volume percentage by 14% in the exfoliated nylon 6/nanoclay system. However, only a 5% volume reduction was observed in the intercalated PS/nanoclay nanocomposites containing 4 wt % nanoclay.[62−64]

In all aPA/organoclay systems used in this study, at similar filler loadings (i.e., 5 wt % MMT), the increased volume percentages of constrained region (< 9%) are much less than those of nylon 6/clay and latex/clay systems (30 and 50% respectively) but are quite close to that of PS/nanoclay hybrid (5% caused by 4 wt % clay). Therefore, it can be seen that such significant differences in the value of C can be attributed to the nature of the polymer, whether it is amorphous, semicrystalline, or cross-linked rubber.

We propose a model to explain this difference. It is well accepted that the addition of nanoclay will cause a nucleating or epitaxial effect in a semicrystalline polymer matrix.[19,20,37] The size of crystals formed close to the clay platelets is much smaller than that of bulk crystallites in a pure polymer with a similar degree of crystallinity.[6,65] The larger surface area of the smaller crystallites in the nanocomposite will result in more polymer chains being restricted in mobility within the amorphous region.[7] Therefore a dramatic increase in constrained volume has been observed in the semicrystalline polymer system in the presence of nanoscale clay fillers. Scheme 1 illustrates the nature of the constrained region in semicrystalline polymers in the presence of nanoclay. In this model, there are two types of constrained region: (a) those in the proximity of the nanoclay layers (part I in Scheme 1) and (b) those in the proximity of the small crystallites (part II in Scheme 1).[66]

Scheme 2 shows the nature of the constrained region in an amorphous polymer in the presence of nanoclay. The small volume of constrained region is composed of the proximal polymer chains encircling nanosized clay platelets (similar to part I in Scheme 1). Furthermore, the size of clay stacks depends on the filler dispersion in polymer matrix: better dispersion would result in thinner clay layers and higher volume of constrained polymer segments. That is why more constrained region exists in the exfoliated aPA

Scheme 1. Proposed Nature of Constrained Region in Semi-Crystalline Polymer/Clay Nanocomposites As Indicated by I and II[a]

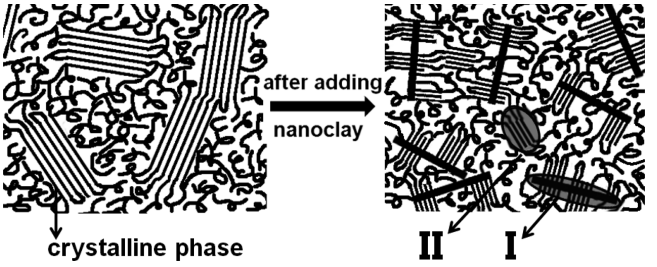

[a] Thick black lines on the right diagram can represent either individual clay platelets or intercalated clay stacks.

Scheme 2. Proposed Nature of Constrained Region in Amorphous Polymer/Clay Nanocomposites As Indicated by I[a]

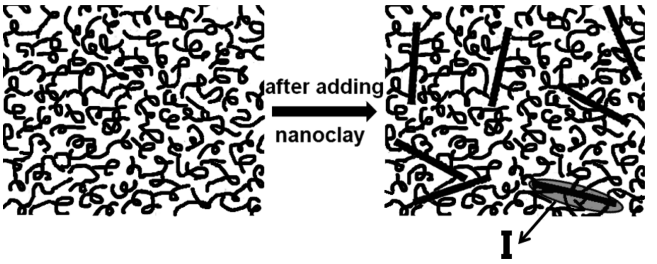

[a] Thick black lines on the right diagram can represent either individual clay platelets or intercalated clay stacks.

nanocomposites than in the intercalated aPA/20AMMT. It indicates that the degree of nanofiller dispersion and interactions between nanoclay and polymer chains are critical in determining the microstructure of the amorphous polymer nanocomposites.[2,42]

It was reported that the crystallization process and crystallite size in cross-linked rubber have been strongly affected by the addition of nanoclay.[28] Therefore, the structural model (Scheme 1) of the constrained region for semicrystalline polymer/nanoclay system is also readily applicable to the cross-linked rubber/nanoclay system.

3.3.4. Relation between Constrained Region and Mechanical Property. It would be appropriate to examine the relationship between our nanoscale constrained region model and the macroscopic mechanical properties of the polymer/clay nanocomposite.[42] Figure 10 shows the graphs of normalized E' at 30 °C versus calculated C and MMT content for the three aPA/organoclay systems. All graphs show that there is very good linear correlation between normalized E' and constrained volume. However, the relationship between storage modulus and MMT content is not as linear, except for aPA/10AMMT.

Because the storage modulus is temperature-dependent,[50] it is also desirable to examine the relationship between E' and the constrained region at other temperatures below the glass transition. Figure 11 shows the graph of normalized E' (at 100 °C) versus constrained volume for the aPA/organoclay systems. It is observed that there is a good linear correlation between storage modulus and constrained volume. Such a linear relationship also exists at other temperatures below T_g. (See the Supporting Information.) At temperatures higher than the glass transition, however, this linear relationship no longer holds because the polymer matrix turns into a viscous state.

On the basis of our proposed model for the nature of the constrained region and the data in Figures 10 and 11, the linear correlation in all aPA/organoclay nanocomposites at a given temperature below the glass transition can be

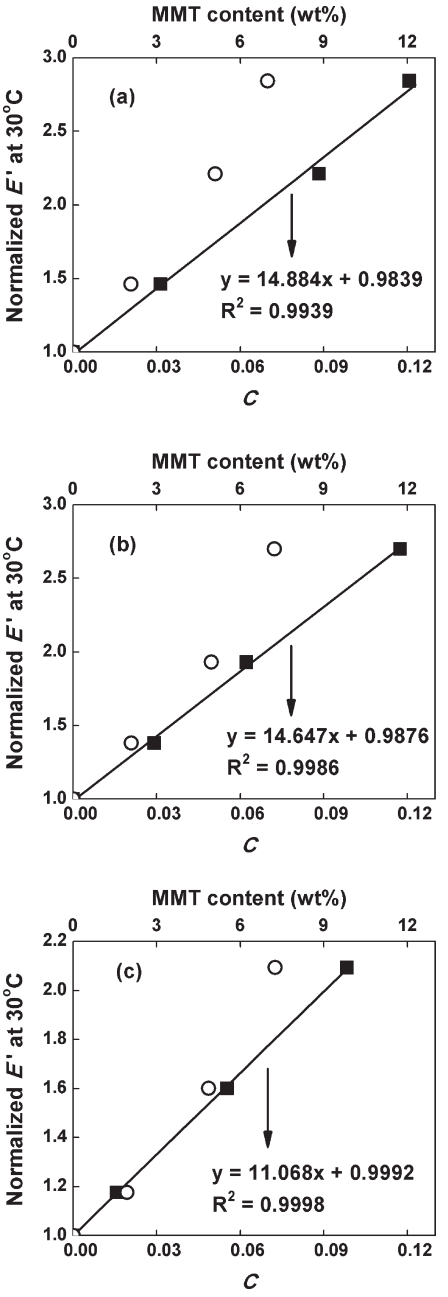

Figure 10. Normalized E' at 30 °C as a function of C (■) and MMT content (○) of (a) aPA/10AMMT, (b) aPA/30BMMT, and (c) aPA/20AMMT nanocomposites. The straight lines are the best fit curves through the constrained volume data points.

expressed as

$$E_n' = E_m'(1-C)+E_c'C \tag{5}$$

where E_n', E_m', and E_c' are the storage modulus of the nanocomposite, the polymer matrix (i.e., aPA), and the constrained region, respectively. It can be seen that eq 5 is basically a "rule of mixtures", similar to the well-defined Takayanagi model for conventional phase-separated composites.[67] In eq 5, the two phases are "polymer matrix" and "constrained region".[27] This equation can be rearranged as follows

$$\frac{E_n'}{E_m'} = \left(\frac{E_c'}{E_m'} - 1\right)C + 1 \tag{6}$$

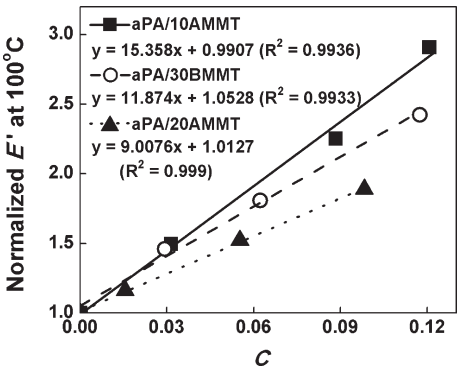

Figure 11. Normalized E' at 100 °C of aPA/organoclay nanocomposites as a function of calculated C. The straight lines are the best fit curves.

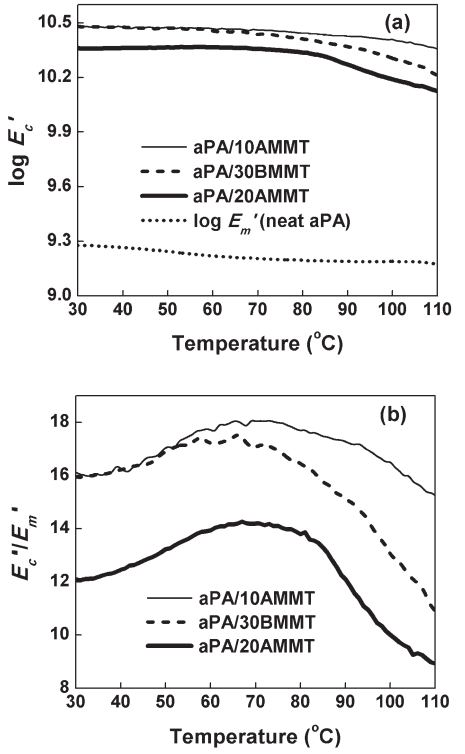

Figure 12. Graphs of (a) constrained volume storage modulus $E_c^{'}$ and (b) the ratios of $E_c^{'}/E_m^{'}$ for all the aPA/organoclay systems from 30 to 110 °C.

which corresponds to the equations of the straight lines observed in Figures 10 and 11. As shown in these Figures, the linear relationship between normalized E' and C indicates that at any given temperature below the glass transition, the ratio $E_c^{'}/E_m^{'}$ for a particular aPA/organoclay system can be considered to be a constant.

Recently, many researchers have applied the Halpin–Tsai–Nielsen model to determine the storage modulus of some polymer nanocomposites.[40,68,69] Our study shows that for a given combination of polymer and organoclay, it is the effect of the constrained region, rather nanoclay content, that controls the enhancement in E'.[7] In semicrystalline systems, Shelley et al. have also observed a similar linear relationship between constrained volume and the room temperature storage modulus in nylon 6/nanoclay nanocomposites.[7] Therefore, the structural model of constrained region can be used effectively to explain and predict the enhanced physical properties not only in semicrystalline polymer/nanoclay systems but also in amorphous polymer/nanoclay systems.

Whereas there have been reports associating constrained region with property enhancement in polymer nanocomposites, there has not been much investigation into the properties of the constrained region.[2,7,27] By using eq 6 and the DMA data, it is possible to determine the value of the storage modulus of the constrained region, $E_c^{'}$, at any given temperature for each aPA/organoclay system. These data are presented in Figure 12.

Figure 12a shows the curves of $E_c^{'}$ for each of the aPA/organoclay systems from 30 to 110 °C. It is observed that the values of $E_c^{'}$ in all systems are much higher (by more than one order of magnitude) than those of $E_m^{'}$ in aPA homopolymer over the entire temperature range. It is not possible to determine the value of $E_c^{'}$ at temperatures near or above T_g because the linear relationship between the storage modulus of the polymer nanocomposite and volume fraction of the constrained region no longer holds in this temperature range.

Furthermore, Figure 12a also shows that in the intercalated aPA/20AMMT system, the value of $E_c^{'}$ is lower than those in the exfoliated aPA/30BMMT and aPA/10AMMT nanocomposites. The value of $E_c^{'}$ in the aPA/30BMMT system is very close to that in the aPA/10AMMT system at temperatures below 80 °C. However, at higher temperatures, $E_c^{'}$ of aPA/30BMMT is much lower than aPA/10AMMT. For all three nanocomposite systems, the value of $E_c^{'}$ is fairly constant at low temperatures up to 80 °C, beyond which $E_c^{'}$ starts to decrease with increasing temperature.

Therefore, it can be seen that the storage modulus of the constrained region is a function of both temperature and polymer–nanoclay interaction. $E_c^{'}$ is lower in nanocomposites with weaker polymer–organoclay interactions (e.g., aPA/20AMMT). Even in the two exfoliated systems, at temperatures above 80 °C, $E_c^{'}$ is higher for aPA/10AMMT, which has stronger polymer–organoclay interactions than aPA/30BMMT. As temperature increases, the interactions between the matrix and nanofiller will be weakened, thus leading to lower values of the constrained region modulus. It is not clear why 80 °C appears to be the "magic number" at which there is an appreciable drop in $E_c^{'}$ for all the three systems studied. Furthermore, $E_c^{'}$ is also expected to depend on filler aspect ratio and orientation. Further research is needed to investigate these issues.

Figure 12b shows the ratio of the storage modulus of the constrained region to that of the polymer matrix, $E_c^{'}/E_m^{'}$, for all three aPA/organoclay systems as a function of temperature below the glass transition. All three curves resemble a parabola with a maximum value located around 70 °C. These data indicate that the reinforcement effect of the constrained region in the polymer nanocomposite is also temperature-dependent. This is attributed to the difference in temperature dependence of the storage modulus for the polymer matrix and the constrained region. At temperatures lower than 70 °C, Figure 12a shows that the matrix modulus decreases appreciably with temperature. This leads to the ratio $E_c^{'}/E_m^{'}$ increasing with temperature up to 70 °C. At temperatures higher than 70 °C, the matrix modulus drops more gradually compared with the large drop in $E_c^{'}$ starting at 80 °C, thereby causing the ratio $E_c^{'}/E_m^{'}$ to decrease with temperature.

Inherent in the proposed model is the fact that the amount of constrained region does not change at temperatures below the glass transition.[27] As long as the polymer matrix is in the glassy state, the polymer–filler interactions (and hence $E_c^{'}$) may change in magnitude depending on the temperature, but the amount of such constrained chains remains the same.

However, at temperatures higher than T_g, the polymer chains have greater mobility, and the constrained volume is expected to vary with temperature under such dynamic conditions.

It is important to note that it is not only the quantity but also the "quality" (i.e., mechanical property) of the constrained region that will determine the eventual mechanical property of the nanocomposite. The key here is really the polymer−organoclay interaction: stronger interaction leads to better dispersion, larger amount of constrained region, larger modulus of the constrained region, and ultimately larger nanocomposite modulus. For instance, in the aPA/20AMMT nanocomposite, there are two factors that contribute to its inferior mechanical properties (compared with the two exfoliated systems). The first factor is the low amount of constrained region due to the intercalated morphology; the second is the lower storage modulus of the constrained region, which is the result of poorer polymer−organoclay interaction. Similarly, we can also see why even though the modulus of the constrained region of aPA/30BMMT is quite close to aPA/10AMMT at 30 °C, the storage modulus of the nanocomposite is larger for the latter. This is because at any given MMT content, there is a larger amount of constrained region in aPA/10AMMT compared with that in aPA/30BMMT. Therefore, both the quantity and the magnitude of the storage modulus of the constrained region for each particular nanocomposite system must be taken into consideration when determining its property.

4. Conclusions

We have examined in detail the structure−property relationship of a polymer/layered nanocomposite system. By removing the complications due to semicrystalline regions, we have been able to investigate the role and nature of constrained region as the reinforcement mechanism. The type of polymer−nanofiller interaction strongly influences the amount and modulus of the constrained region, and both of the latter contribute to the enhancement in the storage modulus of the polymer nanocomposite. The mechanical property and reinforcement effect of the constrained region have also been found to be temperature-dependent. DMA is deemed to be a suitable technique for obtaining pertinent information for the constrained volume.

Constrained region models have been proposed for polymer nanocomposites based on semicrystalline polymers and on amorphous polymers. It is found the amount of constrained volume also depends on the nature of the polymer: semicrystalline, cross-linked rubber, or amorphous. The latter contains the least amount of constrained volume compared with semicrystalline or rubbery systems. This would have important implications in the relative role of nanofillers in the design of polymer nanocomposites with enhanced properties (e.g., HDT, etc.).

Acknowledgment. The work was sponsored by a grant from Nanyang Technological University. We thank Prof. Mary Chan and Dr. Xiujuan Wang for the use of their materials and equipment.

Supporting Information Available: Normalized E' at 55 and 80 °C of aPA/organoclay nanocomposites as a function of calculated C. This material is available free of charge via the Internet at http://pubs.acs.org.

References and Notes

(1) Fornes, T. D.; Hunter, D. L.; Paul, D. R. *Macromolecules* **2004**, *37*, 1793–1798.
(2) Rao, Y. Q.; Pochan, J. M. *Macromolecules* **2007**, *40*, 290–296.
(3) Zax, D. B.; Yang, D. K.; Santos, R. A.; Hegemann, H.; Giannelis, E. P.; Manias, E. *J. Chem. Phys.* **2000**, *112*, 2945–2951.
(4) Fornes, T. D.; Yoon, P. J.; Keskkula, H.; Paul, D. R. *Polymer* **2001**, *42*, 9929–9940.
(5) Kojima, Y.; Usuki, A.; Kawasumi, M.; Okada, A.; Kurauchi, T.; Kamigaito, O. *J. Polym. Sci., Part A: Polym. Chem.* **1993**, *31*, 1755–1758.
(6) Kojima, Y.; Usuki, A.; Kawasumi, M.; Okada, A.; Kurauchi, T.; Kamigaito, O. *J. Appl. Polym. Sci.* **1993**, *49*, 1259–1264.
(7) Shelley, J. S.; Mather, P. T.; DeVries, K. L. *Polymer* **2001**, *42*, 5849–5858.
(8) Vaia, R. A.; Sauer, B. B.; Tse, O. K.; Giannelis, E. P. *J. Polym. Sci., Part B: Polym. Phys.* **1997**, *35*, 59–67.
(9) Lu, H. B.; Nutt, S. *Macromolecules* **2003**, *36*, 4010–4016.
(10) Tran, T. A.; Said, S.; Grohens, Y. *Macromolecules* **2005**, *38*, 3867–3871.
(11) Vyazovkin, S.; Dranca, I. *J. Phys. Chem. B* **2004**, *108*, 11981–11987.
(12) Lee, K. M.; Han, C. D. *Polymer* **2003**, *44*, 4573–4588.
(13) Dai, X. H.; Xu, J.; Guo, X. L.; Lu, Y. L.; Shen, D. Y.; Zhao, N.; Luo, X. D.; Zhang, X. L. *Macromolecules* **2004**, *37*, 5615–5623.
(14) Liu, Z. S.; Erhan, S. Z.; Xu, J. Y. *Polymer* **2005**, *46*, 10119–10127.
(15) Krishnamoorti, R.; Vaia, R. A.; Giannelis, E. P. *Chem. Mater.* **1996**, *8*, 1728–1734.
(16) Park, J.; Jana, S. C. *Macromolecules* **2003**, *36*, 8391–8397.
(17) Pramoda, K. P.; Liu, T. X. *J. Polym. Sci., Part B: Polym. Phys.* **2004**, *42*, 1823–1830.
(18) Park, J.; Jana, S. C. *Polymer* **2004**, *45*, 7673–7679.
(19) Maiti, P.; Nam, P. H.; Okamoto, M.; Hasegawa, N.; Usuki, A. *Macromolecules* **2002**, *35*, 2042–2049.
(20) Kojima, Y.; Usuki, A.; Kawasumi, M.; Okada, A.; Kurauchi, T.; Kamigaito, O.; Kaji, K. *J. Polym. Sci., Part B: Polym. Phys.* **1995**, *33*, 1039–1045.
(21) Li, Y. Q.; Ishida, H. *Macromolecules* **2005**, *38*, 6513–6519.
(22) Panek, G.; Schleidt, S.; Mao, Q.; Wolkenhauer, M.; Spiess, H. W.; Jeschke, G. *Macromolecules* **2006**, *39*, 2191–2200.
(23) Jang, B. N.; Wang, D. Y.; Wilkie, C. A. *Macromolecules* **2005**, *38*, 6533–6543.
(24) Ratinac, K. R.; Gilbert, R. G.; Ye, L.; Jones, A. S.; Ringer, S. P. *Polymer* **2006**, *47*, 6337–6361.
(25) Colombini, D.; Maurer, F. H. J. *Macromolecules* **2002**, *35*, 5891–5902.
(26) Wang, K.; Liang, S.; Deng, J. N.; Yang, H.; Zhang, Q.; Fu, Q.; Dong, X.; Wang, D. J.; Han, C. C. *Polymer* **2006**, *47*, 7131–7144.
(27) Kojima, Y.; Usuki, A.; Kawasumi, M.; Okada, A.; Fukushima, Y.; Kurauchi, T.; Kamigaito, O. *J. Mater. Res.* **1993**, *8*, 1185–1189.
(28) Burnside, S. D.; Giannelis, E. P. *J. Polym. Sci., Part B: Polym. Phys.* **2000**, *38*, 1595–1604.
(29) Adame, D.; Beall, G. W. *Appl. Clay Sci.* **2009**, *42*, 545–552.
(30) Zhang, X.; Loo, L. S. *J. Polym. Sci., Part B: Polym. Phys.* **2008**, *46*, 2605–2617.
(31) Paul, D. R.; Bucknall, C. B. In *Polymer Blends*; Wiley: New York, 2000; Vol. *2*, pp 336−338.
(32) Hodge, I. M. *J. Non-Cryst. Solids* **1994**, *169*, 211–266.
(33) Danch, A.; Osoba, W. *J. Therm. Anal. Calorim.* **2004**, *78*, 923–932.
(34) Hu, Y. S.; Mehta, S.; Schiraldi, D. A.; Hiltner, A.; Baer, E. *J. Polym. Sci., Part B: Polym. Phys.* **2005**, *43*, 1365–1381.
(35) Lincoln, D. M.; Vaia, R. A.; Krishnamoorti, R. *Macromolecules* **2004**, *37*, 4554–4561.
(36) Nair, S. S.; Ramesh, C. *Macromolecules* **2005**, *38*, 454–462.
(37) Shah, D.; Maiti, P.; Gunn, E.; Schmidt, D. F.; Jiang, D. D.; Batt, C. A.; Giannelis, E. R. *Adv. Mater.* **2004**, *16*, 1173–1177.
(38) Ash, B. J.; Siegel, R. W.; Schadler, L. S. *Macromolecules* **2004**, *37*, 1358–1369.
(39) Skrovanek, D. J.; Howe, S. E.; Painter, P. C.; Coleman, M. M. *Macromolecules* **1985**, *18*, 1676–1683.
(40) Okamoto, M.; Morita, S.; Kim, Y. H.; Kotaka, T.; Tateyama, H. *Polymer* **2001**, *42*, 1201–1206.
(41) Chen, J. S.; Poliks, M. D.; Ober, C. K.; Zhang, Y. M.; Wiesner, U.; Giannelis, E. *Polymer* **2002**, *43*, 4895–4904.
(42) Miltner, H. E.; Assche, G. V.; Pozsgay, A.; Pukaszky, B.; Mele, B. V. *Polymer* **2006**, *47*, 826–835.
(43) Donth, E. J. In *The Glass Transition: Relaxation Dynamics in Liquids and Disordered Materials*; Springer: Berlin, 2001; pp 158−159.
(44) Chua, Y. C.; Lu, X. H. *Langmuir* **2007**, *23*, 1701–1710.
(45) Cowie, J. M. G. In *Polymers: Chemistry and Physics of Modern Materials*, 3rd ed.; CRC Press: Boca Raton, FL, 2007; pp 337−338.

(46) Winberg, P.; Eldrup, M.; Pedersen, N. J.; van Es, M. A.; Maurer, F. H. J. *Polymer* **2005**, *46*, 8239–8249.
(47) Chen, K.; Wilkie, C. A.; Vyazovkin, S. *J. Phys. Chem. B* **2007**, *111*, 12685–12692.
(48) Satapathy, B. K.; Weidisch, R.; Potschke, P.; Janke, A. *Compos. Sci. Technol.* **2007**, *67*, 867–879.
(49) Fornes, T. D.; Paul, D. R. *Polymer* **2003**, *44*, 4993–5013.
(50) Wilkinson, A. N.; Man, Z.; Stanford, J. L.; Matikainen, P.; Clemens, M. L.; Lees, G. C.; Liauw, C. M. *Macromol. Mater. Eng.* **2006**, *291*, 917–928.
(51) Manias, E.; Touny, A.; Wu, L.; Strawhecker, K.; Lu, B.; Chung, T. C. *Chem. Mater.* **2001**, *13*, 3516–3523.
(52) Chisholm, B. J.; Moore, R. B.; Barber, G.; Khouri, F.; Hempstead, A.; Larsen, M.; Olson, E.; Kelley, J.; Balch, G.; Caraher, J. *Macromolecules* **2002**, *35*, 5508–5516.
(53) Ke, Y. C.; Long, C. F.; Qi, Z. N. *J. Appl. Polym. Sci.* **1999**, *71*, 1139–1146.
(54) Rao, Y.; Blanton, T. N. *Macromolecules* **2008**, *41*, 935–941.
(55) Nielsen, L. E.; Landel, R. F. In *Mechanical Properties of Polymers and Composites*, 2nd ed.; Marcel Dekker: New York, 1994; pp 436−437, 141−142.
(56) Ratna, D.; Divekar, S.; Samui, A. B.; Chakraborty, B. C.; Banthia, A. K. *Polymer* **2006**, *47*, 4068–4074.
(57) Abdalla, M.; Dean, D.; Adibempe, D.; Nyairo, E.; Robinson, P.; Thompson, G. *Polymer* **2007**, *48*, 5662–5670.
(58) Zhao, J.; Wang, J. J.; Li, C. X.; Fan, Q. R. *Macromolecules* **2002**, *35*, 3097–3103.
(59) Vigier, G.; Tatibouet, J.; Benatmane, A.; Vassoille, R. *Colloid Polym. Sci.* **1992**, *270*, 1182–1187.
(60) Unpublished data.
(61) Coleman, M. M.; Skrovanek, D. J.; Hu, J. B.; Painter, P. C. *Macromolecules* **1988**, *21*, 59–65.
(62) Simha, R.; Utracki, L. A.; Garcia-Rejon, A. *Compos. Interfaces* **2001**, *8*, 345–353.
(63) Utracki, L. A.; Simha, R.; Garcia-Rejon, A. *Macromolecules* **2003**, *36*, 2114–2121.
(64) Tanoue, S.; Utracki, L. A.; Garcia-Rejon, A.; Tatibouet, J.; Cole, K. C.; Kamal, M. R. *Polym. Eng. Sci.* **2004**, *44*, 1046–1060.
(65) Strawhecker, K. E.; Manias, E. *Macromolecules* **2001**, *34*, 8475–8482.
(66) Boyd, R. H.; Smith, G. D. In *Polymer Dynamics and Relaxation*; Cambridge: New York, 2007; p 197.
(67) Arridge, R. G. C. In *An Introduction to Polymer Mechanics*; Taylor & Francis: London, 1985; pp 131−132.
(68) Nam, P. H.; Maiti, P.; Okamoto, M.; Kotaka, T.; Hasegawa, N.; Usuki, A. *Polymer* **2001**, *42*, 9633–9640.
(69) Brune, D. A.; Bicerano, J. *Polymer* **2002**, *43*, 369–387.